AIAA JOURNAL
Vol. 45, No. 3, March 2007

Aeroelastic Analysis of Bearingless Rotors Using Large Deflection Beam Theory

In-Gyu Lim* and In Lee†
Korea Advanced Institute of Science and Technology, Daejeon 305-701, Republic of Korea

DOI: 10.2514/1.26635

The aeroelastic response and stability of bearingless rotors are investigated using large deflection beam theory. The bearingless rotor configuration consists of a single flexbeam with a wraparound-type torque tube and pitch links located at the leading edge and trailing edge of the torque tube. The outboard main blade, flexbeam, and torque tube are all assumed to be an elastic beam undergoing arbitrary large displacements and rotations, which are discretized into beam finite elements. The finite element equations of motion for beams are obtained from Hamilton's principle. Two-dimensional quasi-steady strip theory is used to evaluate aerodynamic forces in both hover and forward flight. For the analysis of hover flight, the nonlinear equations of motion are solved for an equilibrium position through an iterative procedure. The modal approach method based on coupled rotating natural modes is used for the stability analysis. For the analysis of forward flight, the nonlinear periodic blade steady response is obtained by integrating the full finite element equation in time through a coupled trim procedure with a vehicle trim. After the coupled trim response is computed, the aeroelastic response is calculated through a time-marching solution procedure under small perturbations assumption. A stability analysis is then performed using a moving block analysis. The results of the full finite element analysis using the large deflection beam theory are quite different from those of a previously published modal analysis using the moderate deflection-type beam theory.

Nomenclature

a_0	=	two-dimensional lift curve slope
C_T	=	thrust coefficient $[T/\rho_a \pi R^2 (\Omega R)^2]$
e_1, e_2, e_3	=	reference orthogonal unit vectors in the undeformed configuration
e_1^*, e_2^*, e_3^*	=	reference orthogonal unit vectors in the deformed configuration
$\bar{e}_{11}, \bar{e}_{12}, \bar{e}_{13}$	=	strain vectors at reference point
i_1, i_2, i_3	=	rotating hub fixed orthogonal unit vectors
k_1, k_2, k_3	=	strain curvature vectors in the undeformed configuration
q	=	generalized nodal displacement vector
$T(x_1)$	=	transformation matrix between deformed blade axis and rotating hub axis
$t_e(x_1)$	=	transformation matrix between undeformed blade axis and deformed blade axis
$t_g(x_1)$	=	transformation matrix between undeformed blade axis and rotating hub axis
u, v, w	=	elastic displacements in x-, y-, and z-directions, respectively
w_1, w_2, w_3	=	warping displacements
α_s, ϕ_s	=	longitudinal and lateral shaft tilt angles, deg
γ	=	lock number $(3\rho acR/m_0)$
$\theta_{75}, \theta_{1c}, \theta_{1s}$	=	collective, lateral, longitudinal cyclic pitch angles, deg
λ_i	=	induced inflow ratio
μ	=	advance ratio
σ	=	blade solidity $(N_b c/\pi R)$
ψ	=	azimuth angle, Ωt

Subscript

$,i$	=	$\partial(\,)/\partial x_i,\ i = 2, 3$

Superscripts

$'$	=	$\partial(\,)/\partial x_1$
$\cdot$	=	$\partial(\,)/\Omega\partial t = \partial(\,)/\partial\psi$

I. Introduction

IN RECENT years there has been growing interest in the bearingless rotor, because of its design simplicity, enhanced control power, and easy maintenance. A bearingless rotor is one example of a hingeless rotor in which the pitch bearing, flap, and lag hinges are eliminated. The bearingless configuration shown in Fig. 1 consists of a single flexbeam with a wraparound-type torque tube with the pitch links located at the leading or trailing edge of the torque tube and main blade. The distinguishing features of the bearingless rotor are torsionally soft flexbeam and torsionally stiff torque tube. Pitch control to the main blade is applied through a torque tube by rotating it with pitch links, which in turn twists the flexbeam. In general, the aeroelastic stability of a rotor blade is inherently a nonlinear phenomenon. The analysis of a bearingless rotor blade is more complicated than that of a hingeless rotor blade because of the redundancy of load paths at the root and nonlinear bending–torsion coupling effects.

Generally, studies on rotor blades have been performed for global deformation and cross-sectional analyses. One-dimensional global deformation analyses of rotor blades with consideration of the geometrical nonlinearity have been classified into two types of beam theory: moderate deflection and a large deflection. Most of the structural dynamic models for rotor blades are based on moderate deflection-type beam theories. These theories are based on ordering schemes and are valid for moderate deflections [1]. In the literature, some attempts to analyze the stability of bearingless rotors using the moderate deflection-type beam theory have been reported. Hodges [2] developed an analysis [flexbeam air resonance (FLAIR)] to calculate ground and air resonance of bearingless rotors in hover. Each blade was assumed to be rigid, and was attached to the hub through a single uniform flexible beam. Quasi-steady aerodynamics was used. The fuselage was considered as a rigid body with 4 degrees of freedom: longitudinal and lateral translations, and body pitch and

Received 19 July 2006; revision received 7 December 2006; accepted for publication 4 November 2006.

*Graduate Research Assistant, Department of Aerospace Engineering, 373-1 Guseong-dong, Yuseong-gu.

†Professor, Department of Aerospace Engineering, 373-1 Guseong-dong, Yuseong-gu (corresponding author). Associate Fellow AIAA.

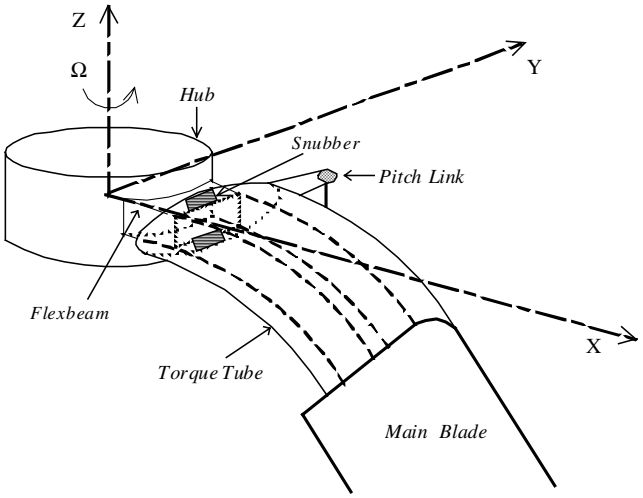

Fig. 1 Bearingless rotor blade configuration.

roll modes. An iterative procedure was adopted to calculate the nonlinear equilibrium position of the flexbeam and a perturbation approach was used to predict the stability. Hodges [3] compared results from the theory of [2] with wind tunnel measurements on a bearingless rotor model. The blade consisted of twin-C-flexbeams and a torque rod.

Meanwhile, Dawson [4] conducted a hover test of a model bearingless rotor with regard to aeroelastic stability to verify the predictions of Hodges [2]. The rotor had a single flexbeam with an external torque tube. The influence of pitch–flap coupling was examined by varying the radial location of the pitch arm. Sivaneri and Chopra [5] applied a finite element formulation to analyze the aeroelastic stability of a bearingless rotor in hover. Each of the flexbeams and the torque tube were modeled as an individual elastic beam. The displacement compatibility conditions at the clevis, between the inboard flexure beams and the outboard blade, were satisfied. The results showed that a multiple load-path blade root cannot be represented by an equivalent single beam. It was shown that the frequently adopted equivalent beam representation for a bearingless rotor blade can lead to erroneous results. Chopra [6] calculated the aeroelastic stability for a bearingless circulation control rotor model in hover using the finite element analysis of [5]. A correlation study of analytical results with the experimental data was also attempted for selected bearingless rotor blade configurations with conventional airfoil characteristics taken from [4]. Chopra [7] examined the aeroelastic stability of the aforementioned rotors in forward flight. The nonlinear steady blade response was calculated from an iterative procedure based on Floquet theory, and stability of perturbation motion was determined from Floquet transition matrix theory. The effects of several design parameters on blade stability were also examined. Hooper [8] modified the analysis of Hodges [2] to include a nonuniform flexbeam as well as another bearingless configuration with a vertical offset of the cuff snubber attachment point to the hub. A systematic parametric study was conducted to examine the influence of several design variables on the aeromechanical stability of this bearingless rotor. Dull and Chopra [9] developed a finite element formulation to analyze the aeroelastic stability of bearingless rotors in forward flight. The nonlinear finite element equations were transformed to a normal mode equation, and these were then solved for the steady response using a time finite element method. Stability results were calculated and correlated with measured data obtained from stability tests of a model rotor in the wind tunnel.

A general purpose analysis, however, demands a large deflection model without any artificial restrictions on displacements or rotations due to the deformation and the degree of nonlinearity. The ordering scheme, although a valuable tool in special purpose research, is not desirable in a general purpose approach. To overcome the limitations of previous models, structural models that are valid for large deflection and are not based on ordering schemes have been developed and used for static [10–17] and dynamic [18–20] analyses of composite beams. The only restriction on the deformation in these theories is that the strain is relatively small compared with unity. There are no small angle approximations made, and all kinematic nonlinear effects are included in the formulation. To date, there have been relatively few studies on aeroelastic analysis of rotor blades using large deflection-type beam theories, and this type of beam theory has only been applied to hingeless rotor blades [21–23].

In this paper, the finite element approach using large deflection-type beam theory is presented for the aeroelastic stability analysis of bearingless rotors in hover and forward flight. The structural model used in the present analysis is modified from Bauchau and Hong's beam model [11]. The aerodynamic forces are modeled using a two-dimensional quasi-steady strip [24]. Nonlinear, periodic blade steady responses are obtained using Borri's time finite element method [25] on a full finite element equation in the forward-flight condition. Blade responses fully coupled with vehicle trim are solved to obtain the nonlinear blade response, pilot controls $(\theta_{75}, \theta_{1c}, \theta_{1s})$, and vehicle attitude (α_s, ϕ_s). Assuming blade motions to be small perturbations about nonlinear periodic equilibrium positions, the aeroelastic response is determined through a time-marching solution procedure. A stability analysis is then performed using a moving block analysis. The full finite element results using the large deflection-type beam theory are compared with the results obtained by a modal approach using the moderate deflection-type beam theory.

II. Analysis

A. Structural Model

Consider the rotor blade rotating with angular velocity Ω depicted in Fig. 2. Here the triad I_1, I_2, and I_3 is fixed in an inertia frame, the triad i_1, i_2, and i_3 fixed in a reference frame that rotates with respect to the inertia frame at a constant angular velocity ΩI_3, the triad e_1, e_2, and e_3 attached to a reference line along the axis of the undeformed blade, and the triad e_1^*, e_2^*, and e_3^* attached to a reference line along the axis of the deformed blade. The geometrical nonlinearities are described using coordinate transformation matrices with the Euler angles in the present large deflection-type beam theory.

$$e_i^* = t_e(x_1)e_i = T(x_1)i_i \qquad T(x_1) = t_e(x_1)t_g(x_1) \tag{1}$$

The transformation matrices t_g, t_e, and T are functions of the curvilinear axial coordinate x_1. Assuming that initial curvatures are small and shearing strains are much smaller than unity in the Green–Lagrangian strain components, strain-displacement relations are represented as given in [12]. If we neglect higher-order strain components and initial curvatures and introduce general warping displacements in and out of plane of a cross section, strain-displacement relations can be expressed as follows [21]:

$$\varepsilon_{11} = \bar{e}_{11} + x_3\kappa_2 - x_2\kappa_3 + w_1' \qquad \gamma_{12} = 2\bar{e}_{12} - x_3\kappa_1 + w_2' + w_{1,2}$$
$$\gamma_{13} = 2\bar{e}_{13} + x_2\kappa_1 + w_3' + w_{1,3} \qquad \varepsilon_{22} = w_{2,2}$$
$$\gamma_{23} = w_{2,3} + w_{3,2} \qquad \varepsilon_{33} = w_{3,3} \tag{2}$$

where x_1, x_2, and x_3 are the curvilinear coordinates and w_1, w_2, and w_3 are the general warping displacements of an arbitrary point on the cross section. The force strains $(\bar{e}_{11}, 2\bar{e}_{12}, 2\bar{e}_{13})$ and moment strains $(\kappa_1, \kappa_2, \kappa_3)$ components are given in [21].

The equations of motion for a bearingless rotor blade are obtained using Hamilton's principle:

$$\int_{t_1}^{t_2} (\delta U - \delta T - \delta W)\, \mathrm{d}t = 0 \tag{3}$$

where

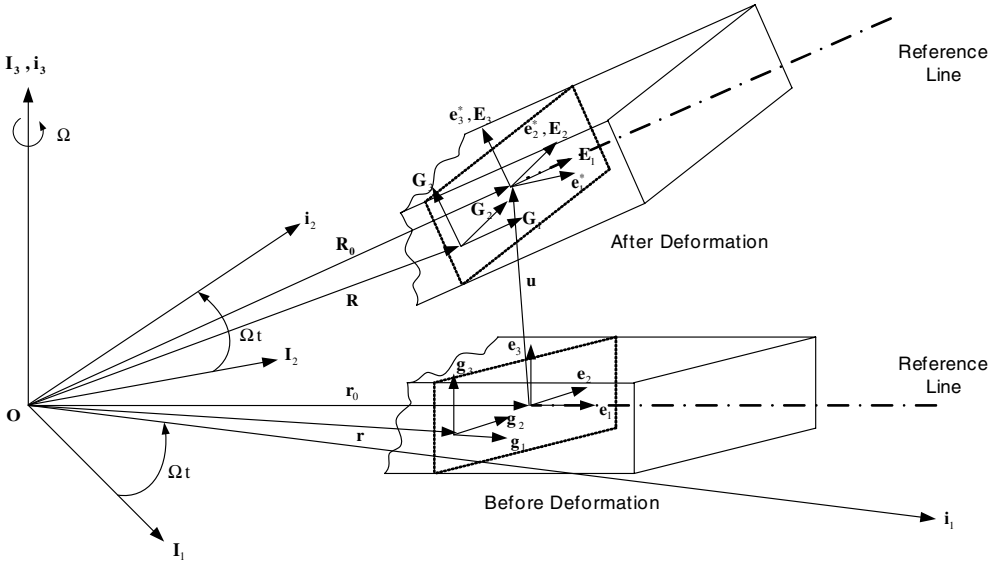

Fig. 2 Geometry and coordinate systems of a rotor blade before and after deformation.

$$\delta U = \int_l \delta \begin{Bmatrix} \bar{e} \\ \bar{\kappa} \end{Bmatrix}^T \begin{bmatrix} A & B \\ B^T & D \end{bmatrix} \begin{Bmatrix} \bar{e} \\ \bar{\kappa} \end{Bmatrix} \mathrm{d}x_1$$

$$\delta T = \int_0^l \int_A \rho \{\delta V\}^T \{V\} \,\mathrm{d}A \,\mathrm{d}x_1 \qquad \delta W = \int_0^l \int_A \delta \{R\}^T \{f\} \,\mathrm{d}A \,\mathrm{d}x_1$$

where δU, δT, and δW are the variation of strain energy given in [20], the variation of kinetic energy, and the virtual work of applied forces, respectively; $\bar{e}$ and $\bar{\kappa}$ vectors are defined as follows: $\bar{e} = \{\bar{e}_{11} \quad 2\bar{e}_{12} \quad 2\bar{e}_{13}\}^T$, $\bar{\kappa} = \{\kappa_1 \quad \kappa_2 \quad \kappa_3\}^T$, and the sectional stiffness matrices A, B, and D are 3×3 matrices that depend not only on the material properties but also on cross-sectional geometry and initial curvature and twists. In the case of isotropic material, these matrices are represented by the diagonal term, ρ is the mass density of the blade, V is the velocity with respect to the inertia frame ($\boldsymbol{V} = \dot{R} + \Omega I_3 \times R$), and f is the external aerodynamic force.

B. Pitch Links Model

Pitch control to the main blade is applied through a torsionally stiff torque tube by rotating it with pitch link, which in turn twists the flexbeam. A pitch link is connected to the root end of the torque tube at its leading or trailing edge. The pitch links model is replaced by spring stiffness. In the global finite element energy expression, the spring contributes an additional strain energy term. When a pitch link is connected at torque tube's leading edge, the added strain energy is

$$U_P = \frac{1}{2} K_P (w_t + \theta_t d)^2 \tag{4}$$

where K_P is the pitch link stiffness, d is pitch link offset from elastic axis, and w_t and θ_t are elastic displacements, respectively.

C. Aerodynamics

In the present work, the aerodynamic lift and pitching moment acting on the blade are obtained by Greenberg's extension [24] of Theodorsen's theory for a two-dimensional airfoil undergoing unsteady motion in an incompressible flow. Two-dimensional quasi-steady strip theory is used to evaluate aerodynamic forces in both hover and forward flight. The components of the resultant velocity U in the deformed blade coordinate system are given by

$$\begin{Bmatrix} U_R \\ U_T \\ U_P \end{Bmatrix} = T \begin{Bmatrix} \dot{u}_1 - \Omega R_{02} - \Omega R \mu \cos\psi \\ \dot{u}_2 + \Omega R_{01} + \Omega R \mu \sin\psi \\ \dot{u}_3 + \Omega R \lambda_i \end{Bmatrix} \tag{5}$$

where $\dot{u}_i$ is the component of the elastic velocity vector $\dot{u}$ of the blade and R_{0i} is the component of the position vector R of an arbitrary point on the cross section in the deformed blade configuration. R is the blade radius, Ω the constant angular velocity, μ the advance ratio, λ_i the inflow ratio, and ψ the azimuth angle of the blade. The advance ratio μ and the inflow ratio λ_i are defined as the nondimensionalized forward speed, $V/\Omega R$, and the induced velocity, $v_{\mathrm{id}}/\Omega R$, respectively. In hover, the induced velocity v_{id} is taken to be steady and uniform along the blade radius and is set equal to the value of inflow given by the combined momentum and blade element theory at a radial station $r = 0.75R$. Thus, the inflow ratio is expressed as

$$\lambda_i = \frac{v_{\mathrm{id}}}{\Omega R} = \frac{\sigma a_0}{16} \operatorname{sign}(\theta_{75}) \left[\sqrt{1 + \frac{24}{\sigma a_0} |\theta_{75}|} - 1 \right] \tag{6}$$

A linear inflow model is used for the rotor inflow distribution in forward flight. For a high advance ratio ($\mu \geq 0.2$), the Drees model is used, whereas for low μ, the White and Blake model [26] is used for comparison with the results of Dull and Chopra [9].

D. Blade Steady Response and Coupled Trim Analysis

In hover, the nonlinear finite element equations of motion in matrix form can be formulated as

$$[M(q)]\{\ddot{q}\} + [G(q)]\{\dot{q}\} + P(q) - P_C(q) = [A(k, q)]\{q\} + P_A(q) \tag{7}$$

where $[M]$, $[G]$, and $[A]$ are the mass, gyroscopic damping, and unsteady aerodynamic matrices in finite elements, respectively. The term P is the internal elastic force vector, P_C is the centrifugal load vector, and P_A is the steady aerodynamic load vector. To solve the governing equation of motion (7), dropping all time-dependent terms, the nonlinear steady-state deformation is calculated through the iterative Newton–Raphson method. In forward flight, the nonlinear, periodic steady response is obtained using a time finite element technique [25]. The virtual energy expression for Hamilton's weak form can be obtained as follows:

$$\int_{\psi_i}^{\psi_f} \delta y^T l \,\mathrm{d}\psi = \delta y^T b \Big|_{\psi_i}^{\psi_f} \tag{8}$$

where

$$\delta y = \begin{Bmatrix} \delta\dot{q} \\ \delta q \end{Bmatrix}; \qquad l = \begin{Bmatrix} L_{\dot{q}} \\ L_q + Q \end{Bmatrix}; \qquad b = \begin{Bmatrix} 0 \\ p \end{Bmatrix} \tag{9}$$

where Q is the generalized forces and L is the Lagrangian of the system. $L_{\dot{q}}$ and L_q are the partial derivatives of L with respect to the generalized coordinates $\dot{q}$ and q, respectively, which are composed

Table 1 Structural properties of elements

Element	Length ℓ/R	Flapwise $EI_y/m_0\Omega^2R^4$	Chordwise $EI_z/m_0\Omega^2R^4$	Torsion $GJ/m_0\Omega^2R^4$	Mass m/m_0	Torsion inertia K_m/R
Torque tube	0.113	4.257	4.257	1.815	7.63	0.0020
Flexbeam	0.084	2.099	2.099	9.150	72.6	0.0346
Flexbeam	0.113	0.00158	0.0052	0.00021	0.299	0.000029
Blade	0.069	0.1216	0.1216	0.2433	39.6	0.0105
Blade	0.734	0.0055	0.1501	0.0029	1.0	0.00091

Table 2 Rotor characteristics for aeroelastic analysis

Radius, m	0.902
Chord/radius C/R	0.0465
Lift coefficient C_l	5.73
Drag coefficient C_d	0.0079
Solidity σ	0.03
Lock number γ	5.9
Pitch link spring stiffness $K_P/m_0\Omega^2R$	171.06
Pitch link offset from elastic axis d/R	0.0409
η_t, η_f	0

of displacements and Euler angles, whereas $p = L_{\dot{q}}$ is the column vector of the generalized moment. ψ_i and ψ_f represent the initial and final states of nondimensionalized time, respectively. Using a first-order Taylor series expansion of the left-hand side of Eq. (8) with respect to a given state vector $\bar{y}$, the following governing equation can be derived in an incremental form:

$$\int_{\psi_i}^{\psi_f} \delta y^T \bar{l}\, \mathrm{d}\psi + \int_{\psi_i}^{\psi_f} \delta y^T \bar{K} \Delta y\, \mathrm{d}\psi = \delta y^T b|_{\psi_i}^{\psi_f} \tag{10}$$

where the local tangent matrix $\bar{K}$ is defined as

$$\bar{K} = \begin{bmatrix} L_{\dot{q}\dot{q}} & L_{\dot{q}q} \\ L_{q\dot{q}} + Q_{\dot{q}} & L_{qq} + Q_q \end{bmatrix} \tag{11}$$

where $L_{\dot{q}\dot{q}}$, $L_{\dot{q}q}$, L_{qq}, $Q_{\dot{q}}$, and Q_q indicate the second and first derivatives with respect to the subscripts, respectively. The time period for one revolution is discretized into a number of time elements with cubic variation. After assembling elements in a global system, a periodic boundary condition is imposed by folding the row and column of the assembled matrix and vector.

The propulsive vehicle trim analysis is fully coupled with the previous blade steady response analysis to solve the blade response, pilot control inputs, and vehicle orientation simultaneously. The vehicle trim solution is calculated from the overall nonlinear vehicle equilibrium equations: three force equations (vertical, longitudinal, and lateral) and three moment equations (pitch, roll, and yaw). However, the yawing moment equilibrium is neglected in this study because the tail rotor is not considered. Fixed frame hub loads are also calculated by summing the contributions from individual blades.

E. Aeroelastic Stability

For the stability analysis in hover, it is assumed that the flutter motion is a small perturbation about the equilibrium position, and the linearized flutter equations are then transformed to the modal space. The transformed modal equations are solved through the p–k modal flutter analysis discussed in [27]. In forward flight, the blade perturbation equations of motion are also linearized about the equilibrium position. The initial value of the perturbed blade motion is taken to be 10% of the equilibrium position. From the initial perturbation, the blade is set free to move and the blade perturbation equations of motion are integrated by the fourth-order Runge–Kutta method. To obtain more accurate modal damping and frequency, the initial perturbation of the blade is given only in the particular mode of interest. After the time histories of the blade lag, flap, and torsional deflections are known, the modal damping and frequency of any desired mode can be determined from the moving block analysis [28].

III. Numerical Results and Discussion

Aeroelastic response and stability analyses of isotropic bearingless rotor blades are performed using the large deflection-type beam theory in hover and forward flight. For the hover analysis, the nonlinear equations of motion are solved for an equilibrium position through an iterative procedure. The modal approach method based on coupled rotating natural modes is used for the stability analysis. For the analysis of forward flight, the nonlinear periodic blade steady response is obtained by integrating the full finite element equation in time through a coupled trim procedure with the vehicle trim. The aeroelastic stability is obtained from time histories

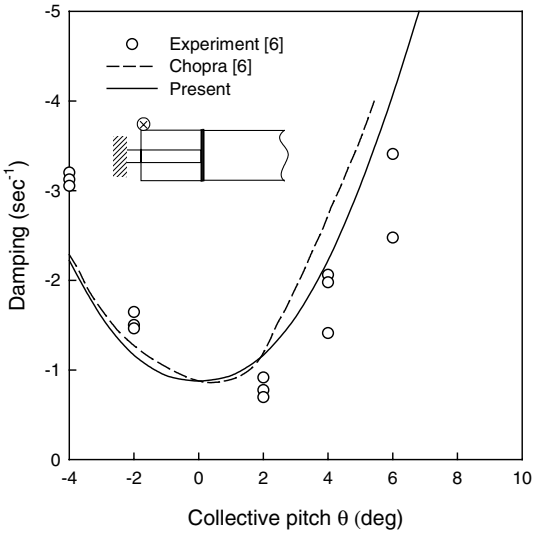

Fig. 3 Lag damping in hover (pitch link at leading edge).

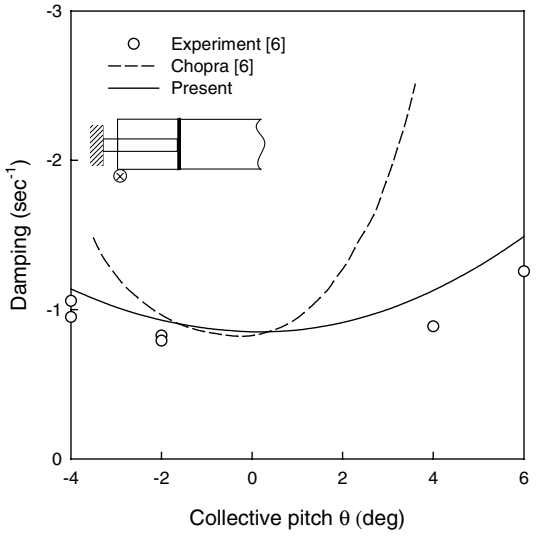

Fig. 4 Lag damping in hover (pitch link at trailing edge).

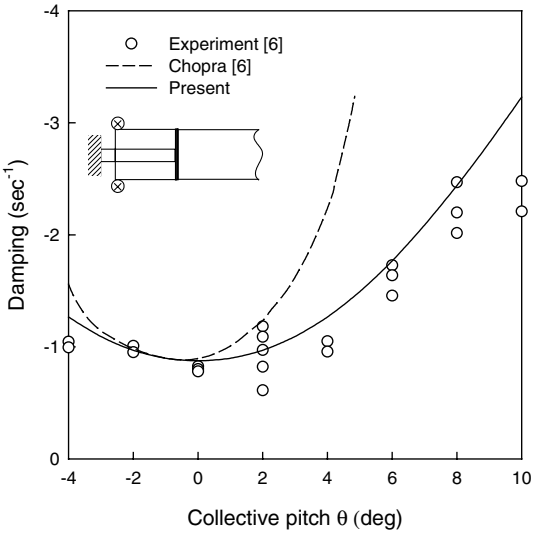

Fig. 5 Lag damping in hover (pitch link at leading and trailing edges).

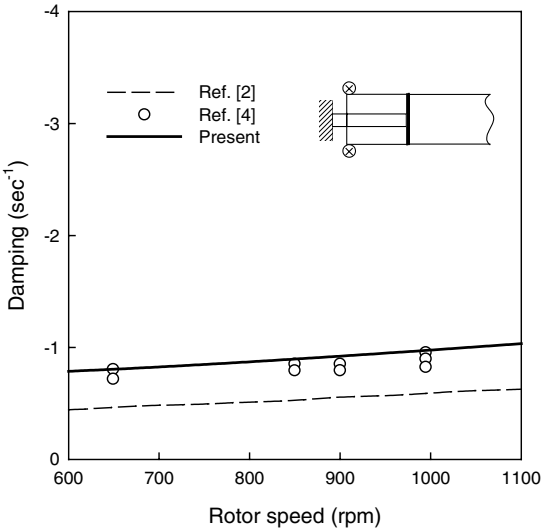

Fig. 7 Lag damping vs rotor speed in hover: $\theta_P = 4$ deg.

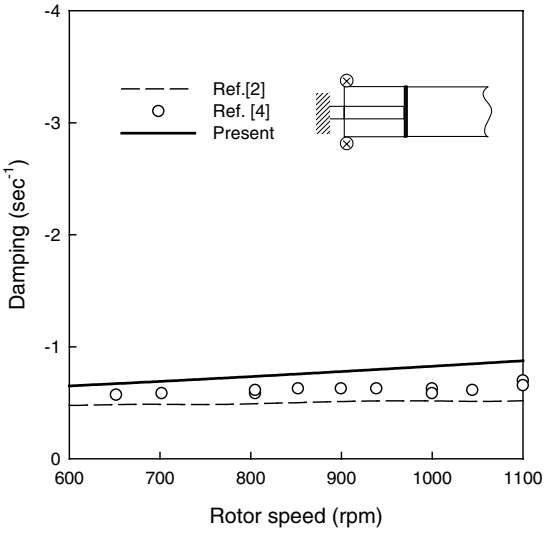

Fig. 6 Lag damping vs rotor speed in hover: $\theta_P = 0$ deg.

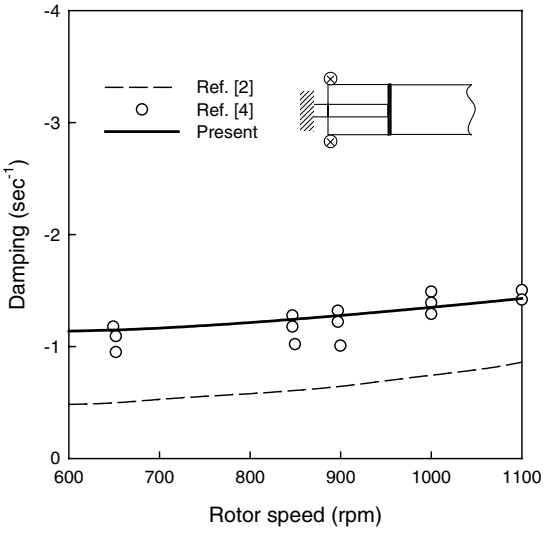

Fig. 8 Lag damping vs rotor speed in hover: $\theta_P = 8$ deg.

of perturbed deflections under a small perturbations assumption about the nonlinear periodic equilibrium position. In the present investigation, the modal analysis using linear rotating vibration modal bases is confirmed to be improper from the poor results obtained in the nonlinear steady response analysis in forward flight. Therefore, the present results obtained by the modal analysis in hover and the full finite element analysis in forward flight using the large deflection-type beam theory are compared with the previous published results obtained by a modal analysis using the moderate deflection-type beam theory. Bauchau and Guernsey [29] noted that the full finite element analysis is preferable for an aeroelastic analysis with coupling of aerodynamics and structural dynamics of helicopter rotor blades. The present paper focuses on investigating nonlinear kinematic effects due to large deflections through a comparison of two models.

A. Aeroelastic Analysis Results in Hover

The flexbeam, torque tube, and main blade are discretized into three, two, and five four-noded cubic elements in the space domain given in [6], respectively. Each of them is modeled as an individual elastic beam. To verify the validity of the present analysis of a bearingless rotor system using large deflection beam theory in hover, the results obtained here are compared with aeroelastic analysis results using moderate deflection beam theory and 2-D quasi-steady aerodynamics and experimental data in hover. The structural properties and the rotor characteristics used for numerical computation are presented in Tables 1 and 2, respectively. Figures 3–5 show the lag damping of the present analysis compared with the existing solution given in [6] as a collective pitch angle with leading-, trailing-, and both-edge pitch link, respectively. This rotor blade is

Table 3 Structural properties of elements

Element	Length ℓ/R	Flapwise $EI_y/m_0\Omega^2R^4$	Chordwise $EI_z/m_0\Omega^2R^4$	Torsion $GJ/m_0\Omega^2R^4$	Mass m/m_0	Torsion inertia K_m^2/R^2
Blade (tip)	0.25	0.00201	0.1049	0.00455	1.0	0.00054
Blade	0.5625	0.00201	0.1049	0.00455	1.0	0.00054
Flexbeam	0.052	0.00004	0.006	0.000055	0.376	0.000032
Flexbeam	0.1147	0.0003	0.015	0.000452	0.870	0.000033
Torque tube	0.0833	0.000246	0.00642	0.00582	0.615	0.000060
Torque tube	0.0833	0.00883	0.01534	0.02967	1.267	0.000031

Table 4 Rotor characteristics for aeroelastic analysis

Number of blades	4
Rotating speed Ω	817 rpm
Solidity σ	0.1079
C_T/σ	0.05
Lock number γ	5.7
Pitch link spring stiffness $K_P/m_0\Omega^2R$	40.0
Pitch link offset from elastic axis d/R	0.0311
Blade prepitch θ_p	9 deg (θ_{75})
Blade linear twist θ_{tw}	−11.3 deg
CG below hub h/R	0.297
Lift coefficient C_l	5.73
Drag coefficient C_d	0.01
Moment coefficient C_m	0.0
Chord/radius c/R	0.08472

straight, untwisted, and installed with no precone. The analysis is conducted with ten elements and seven modes. Figure 3 shows that both the present results and the analysis results in [6] under a rotation of 1100 rpm with a leading-edge pitch link are well correlated with the experimental data at positive collective pitch angles. At negative collective pitch angles, the trend is predicted relatively well. Figure 4 shows the analytic stability results with the experimental data at 900 rpm. The present results are relatively better correlated with the experimental data than the analysis results in [6] at all collective pitch angles. Figure 5 shows the analytic stability results with the experimental data at 1100 rpm. At negative collective pitch angles, the trend is relatively well predicted. The present results are relatively better correlated with the experimental data than the analysis results in [6] at positive collective pitch angles. Figures 6–8 show the lag damping of the present analysis compared with the analysis results in [2] and the experimental data in [4] as a rotor speed with both edge pitch links at different collective pitch angles ($\theta_P = 0$, 4, 8 deg), respectively. The structural properties and the rotor characteristics used for numerical computation are identified in Tables 1 and 2, respectively. Figures 6–8 show that as the rotor speed is increased, the lag damping obtained in the present analysis, as well as that given in [2,4], is gradually augmented. Figure 6 shows that the trend is relatively well predicted. Figures 7 and 8 show that the present results are relatively better correlated with the experimental data than the analysis results in [2] at a high collective pitch angle.

B. Aeroelastic Analysis Results in Forward Flight

The flexbeam, torque tube, and main blade are discretized into two four-noded cubic elements in the space domain, respectively, and the time period of one rotor revolution is discretized into six four-noded cubic elements in the time domain given in [9]. The structural

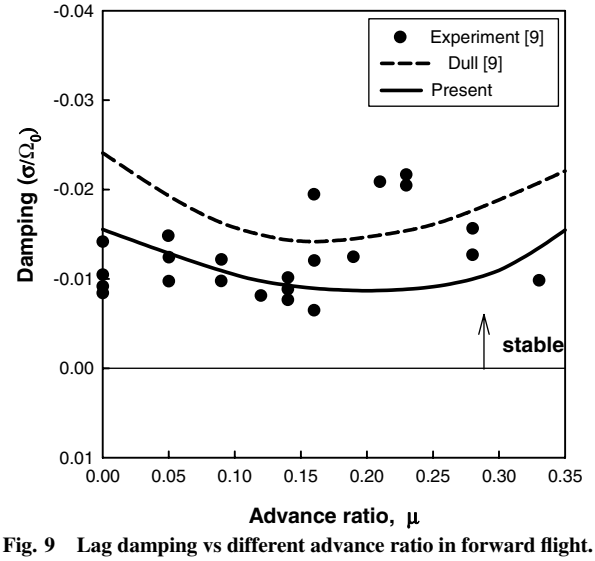

Fig. 9 Lag damping vs different advance ratio in forward flight.

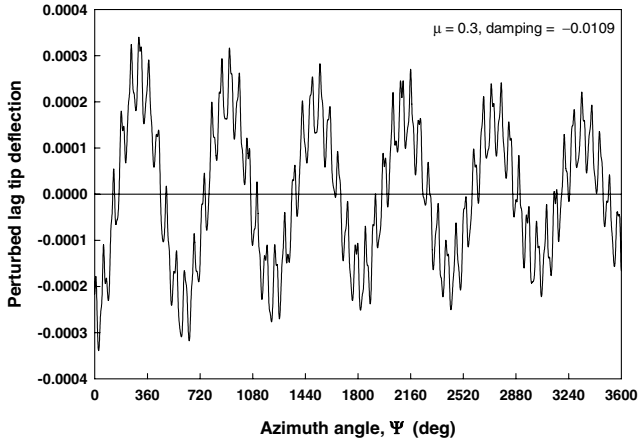

a) Time history of perturbed lag tip deflection

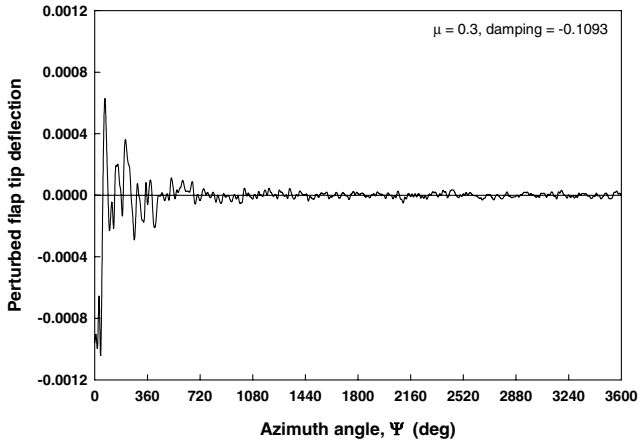

b) Time history of perturbed flap tip deflection

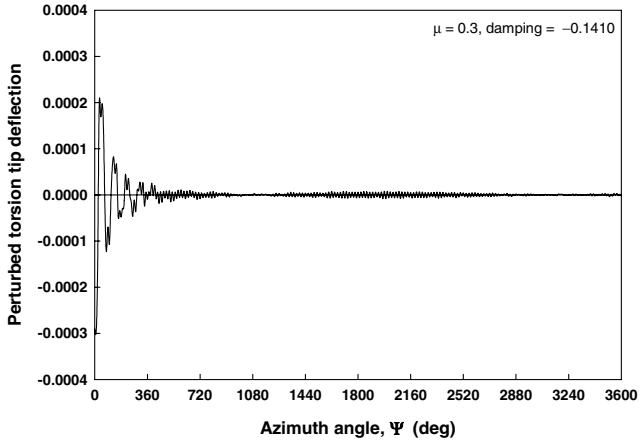

c) Time history of perturbed torsion tip deflection

Fig. 10 Time histories of perturbed motions from initial perturbations ($\mu = 0.3$).

properties and vehicle configuration of the bearingless rotor blade used for numerical computation are presented in Tables 3 and 4. To establish the validity of the present analysis of a bearingless rotor system using large deflection beam theory in forward flight, the obtained results are compared with aeroelastic analysis results using moderate deflection beam theory and 2-D quasi-steady aerodynamics and experimental data in forward flight. Figure 9 shows the lag damping of the present analysis compared with the previous results given in [9] as an advance ratio. The present results are relatively better correlated with the experimental data than the analysis results in [9]. The results of [9] are obtained using a modal analysis with a modal basis of seven coupled rotating natural modes (two flap, two lag, two torsion, and one axial mode) based on the

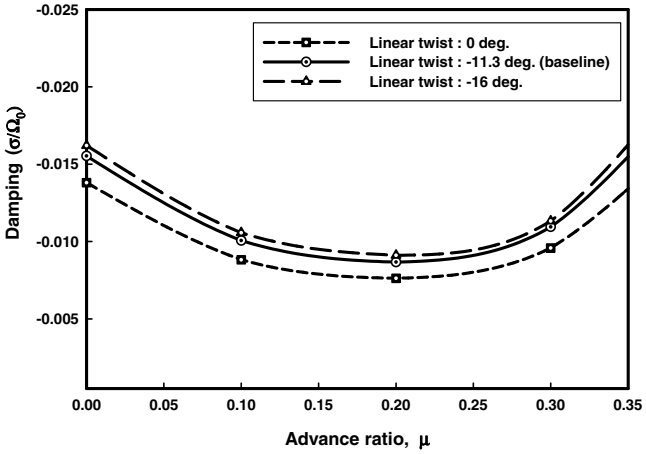

Fig. 11 Effect of blade linear twist on lag damping in forward flight.

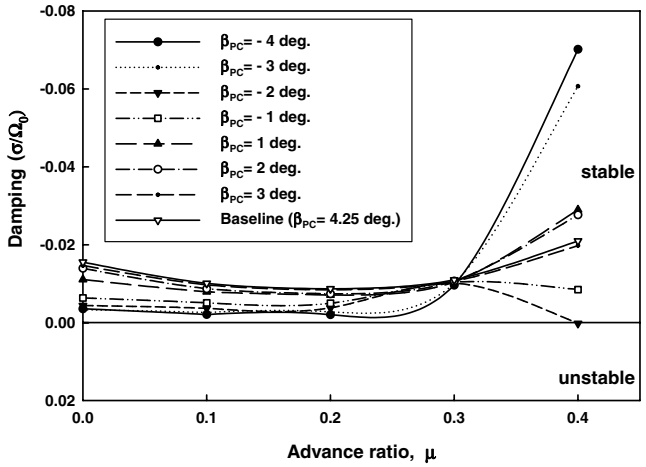

Fig. 12 Effect of hub precone on lag damping in forward flight.

moderate deflection-type beam theory. The present results are obtained using a full finite element analysis based on the large deflection-type beam theory. At high advance ratios, the experimental data are not reliable due to difficulty in trimming the model in the test [9]. Hence, as shown in Fig. 9, the trend between these results is quite similar for low advance ratios but variation in the trends appears at high advance ratios. The modal damping characteristics of the present results are determined through a moving block analysis for the time histories. The time histories for the blade motions are obtained from an initial perturbation about the known periodic equilibrium deflections under a small perturbations assumption in the lag mode. It is observed that the damping obtained from the present analysis generally has a lower value than that of [9] from Floquet theory with a modal basis. Figure 10 shows the time histories for blade motions obtained from an initial perturbation about the known periodic equilibrium deflections under small perturbations assumption. To obtain the time histories of individual modes, the initial perturbation of the blade is given only in the particular mode of interest. The results show that the lag mode damping is the smallest one. The lag mode stability is generally treated as an important factor of aeroelastic stability analysis of rotor blades because the aerodynamic damping of the lag mode is the mildest one. To predict the effect of the various parameters on lag mode stability, a baseline rotor is defined as a verification model (Tables 3 and 4). This baseline rotor is used for comparison in all subsequent results. Figure 11 shows the effect of various blade linear twisting on the baseline rotor. The trend is similar to the baseline rotor but negative blade linear twist is stabilizing at all advance ratios. Figure 12 presents the results for the addition of a positive and negative precone, respectively, to the baseline configuration. The positive precone is more stabilizing than the negative precone at lower advance ratios but destabilizing at higher advance ratios. A special negative precone such as -1 and -2 deg is stabilizing at lower advance ratios but destabilizing at higher advance ratios.

IV. Conclusions

In this paper, the aeroelastic stability of a bearingless rotor in hover and forward flight has been investigated. The finite element analysis is conducted using the large deflection beam model. Numerical results for the lead-lag damping of bearingless rotors correlate very well with existing experimental results. The results using large deflection beam theory show better correlation with experiments than those using moderate deflection beam theory based on the ordering scheme at high pitch angle where the structural modeling, which is valid for large deflections, is required. The nonlinear kinematic effects greatly affect the steady response as the forward speed increases. The aeroelastic modal damping is predicted smaller than that of the modal analysis using the moderate deflection-type beam theory. It is concluded that the full finite element methods using the large deflection-type beam theory should be preferred for the accurate prediction of the bearingless rotor behavior with large deflection. In addition, the effects of negative linear twist and a precone are studied along with an advance ratio.

Acknowledgment

This research was supported by the Brain Korea 21 Project (BK21) in 2006.

References

[1] Rosen, A., and Friedmann, P. P., "The Nonlinear Behavior of Elastic Slender Straight Beams Undergoing Small Strains and Moderate Rotations," *Journal of Applied Mechanics*, Vol. 46, No. 1, 1979, pp. 161–168.

[2] Hodges, D. H., "A Theoretical Technique for Analyzing Aeroelastic Stability of Bearingless Rotors," *AIAA Journal*, Vol. 17, No. 4, 1979, pp. 400–407.

[3] Hodges, D. H., "An Aeromechanical Stability Analysis for Bearingless Rotor Helicopters," *Journal of the American Helicopter Society*, Vol. 24, No. 1, 1979, pp. 2–9.

[4] Dawson, S., "An Experimental Investigation of a Bearingless Model Rotor in Hover," *Journal of the American Helicopter Society*, Vol. 28, No. 4, 1983, pp. 29–34.

[5] Sivaneri, N. T., and Chopra, I., "Finite Element Analysis for Bearingless Rotor Blades Aeroelasticity," *Journal of the American Helicopter Society*, Vol. 29, No. 2, 1984, pp. 42–51.

[6] Chopra, I., "Dynamic Stability of a Bearingless Circulation Control Rotor Blade in Hover," *Journal of the American Helicopter Society*, Vol. 30, No. 4, 1985, pp. 40–47.

[7] Chopra, I., "Dynamic Stability of a Bearingless Circulation Control Rotor Blade in Forward Flight," *Journal of the American Helicopter Society*, Vol. 33, No. 3, 1988, pp. 60–67.

[8] Hooper, N. E., "Parametric Study of the Aeroelastic Stability of a Bearingless Rotor," *Journal of the American Helicopter Society*, Vol. 31, No. 1, 1986, pp. 52–64.

[9] Dull, A. L., and Chopra, I., "Aeroelastic Stability of Bearingless Rotors in Forward Flight," *Journal of the American Helicopter Society*, Vol. 33, No. 4, 1988, pp. 38–46.

[10] Bauchau, O. A., and Hong, C. H., "Large Displacement Analysis of Naturally Curved and Twisted Composite Beams," *AIAA Journal*, Vol. 25, No. 11, 1987, pp. 1469–1475.

[11] Bauchau, O. A., and Hong, C. H., "Nonlinear Composite Beam Theory," *Journal of Applied Mechanics*, Vol. 55, No. 1, 1988, pp. 156–163.

[12] Stemple, A. D., and Lee, S. W., "Large Deflection Static and Dynamic Finite Element Analysis of Composite Beams with Arbitrary Cross Sectional Warping," AIAA Paper 89-1363, 1989, pp. 1788–1798.

[13] Minguet, P., and Dugundji, J., "Experiments and Analysis for Composite Blades Under Large Deflections Part 1: Static Behavior," *AIAA Journal*, Vol. 28, No. 9, 1990, pp. 1573–1579.

[14] Hodges, D. H., "A Mixed Variational Formulation Based on Exact Intrinsic Equations for Dynamics of Moving Beams," *International Journal of Solids and Structures*, Vol. 26, No. 11, 1990, pp. 1253–1273.

[15] Atilgan, A. R., and Hodges, D. H., "Unified Nonlinear Analysis for Nonhomogeneous Anisotropic Beams with Closed Cross Sections," *AIAA Journal*, Vol. 29, No. 11, 1991, pp. 1990–1999.

[16] Hodges, D. H., Shang, X., and Cesnik, C. E. S., "Finite Element Solution of Nonlinear Intrinsic Equations for Curved Composite Beams," *Journal of the American Helicopter Society*, Vol. 41, No. 4, 1996, pp. 313–321.
[17] Cesnik, C. E. S., and Hodges, D. H., "VABS: A New Concept for Composite Rotor Blade Cross-Sectional Modeling," *Journal of the American Helicopter Society*, Vol. 42, No. 1, 1997, pp. 27–38.
[18] Minguet, P., and Dugundji, J., "Experiments and Analysis for Composite Blades Under Large Deflections Part 2: Dynamic Behavior," *AIAA Journal*, Vol. 28, No. 9, 1990, pp. 1579–1588.
[19] Hodges, D. H., Atilgan, A. R., Fulton, M. V., and Rehfield, L. W., "Free-Vibration Analysis of Composite Beams," *Journal of the American Helicopter Society*, Vol. 36, No. 3, 1991, pp. 36–47.
[20] Jeon, S. M., Cho, M. H., and Lee, I., "Static and Dynamic Analysis of Composite Box Beams Using Large Deflection Theory," *Computers and Structures*, Vol. 57, No. 4, 1995, pp. 635–642.
[21] Cho, M. H., and Lee, I., "Aeroelastic Stability of Hingeless Rotor Blade in Hover Using Large Deflection Theory," *AIAA Journal*, Vol. 32, No. 7, 1994, pp. 1472–1477.
[22] Cho, M. H., and Lee, I., "Aeroelatic Analysis of Multibladed Hingeless Rotors in Hover," *AIAA Journal*, Vol. 33, No. 12, 1995, pp. 2348–2353.
[23] Cho, M. H., Jeon, S. M., Woo, S. H., and Lee, I., "Refined Aeroelastic Analysis of Hingeless Rotor Blades in Hover," *Journal of Aircraft*, Vol. 34, No. 3, 1997, pp. 408–415.
[24] Greenberg, J. M., "Airfoil in Sinusoidal Motion in a Pulsating Stream," NACA TN-1326, 1947.
[25] Borri, M., "Helicopter Rotor Dynamics by Finite Element Time Approximations," *Computers and Mathematics with Applications (1975-) / Computers & Mathematics with Applications*, Vol. 12A, No. 1, 1986, pp. 149–160.
[26] White, F., and Blake, B. B., "Improved Method of Predicting Helicopter Control Response and Gust Sensitivity," American Helicopter Society Paper 79-25, May 1979.
[27] Yamane, T., and Friedmann, P. P., "Aeroelastic Tailoring Analysis for Preliminary Design of Advanced Turbo Propellers with Composite Blades," *Journal of Aircraft*, Vol. 30, No. 1, 1993, pp. 119–126.
[28] Hammond, C. E., and Doggett, R. V., Jr., "Determination of Subcritical Damping by Moving-Block/Randomdec Application," *NASA Symposium on Flutter Testing Techniques*, 1975.
[29] Bauchau, O. A., and Guernsey, D., "On the Choice of Appropriate Bases for Nonlinear Dynamic Modal Analysis," *Journal of the American Helicopter Society*, Vol. 38, No. 4, 1993, pp. 28–36.

B. Balachandran
Associate Editor